MOLEKUL
eISSN: 2503-0310

Articles
https://doi.org/10.20884/1.jm.2025.20.2.13578

Metabolomic Profiling LC-MS Based Bioactive Compound of *Sonneratia alba*, Antioxidant Activities and Its In-silico molecular docking Studies

Indra Lasmana Tarigan[1,3], Madyawati Latief[1,3]*, Jamaludin Al-Anshori[2], Fitria Melani[1], Silvi Ayudiah Putri[1], Naimul Husna[1], Tri Warni[1], Ilham Ifandi Ramadhan[1], Yusnaidar[1], Sutrisno[1]

[1]Department of Chemistry, Faculty of Science and Technology, Universitas Jambi, Indonesia
[2]Department of Chemistry, Faculty of Mathematic and Natural Sciences, Universitas Padjajaran, Indonesia
[3]NPBC Laboratory, Faculty of Science and Technology, Universitas Jambi, Indonesia

*Corresponding author email: madyawatilatief@unja.ac.id

Received November 07, 2024; **Accepted** June 10, 2025; **Available online** July 20, 2025

ABSTRACT. Mangrove Perepat (*Sonneratia alba*) plants have various potentials that need to be utilized optimally because they have varying bioactive compound content. A comprehensive exploration of secondary metabolite compound content and plant bioactivity based on metabolomics and in-silico molecular docking is needed to see the effects of single or multiple compounds. This study aimed to obtain a profile of medicinal compounds from Perepat leaves as antioxidants. Extraction was carried out using five gradients of Ethanol: Water concentration. EP1 (water), EP2 (25% Ethanol), EP3 (50% Ethanol), EP4 (75% Ethanol), EP5 (100% Ethanol). The research was carried out through extraction, antioxidant determination, metabolomics, and molecular docking. Exploration data showed that increasing ethanol concentration increased phenolics, flavonoids, and antioxidant activity. EP5 has the highest total phenolics and flavonoids of 24.978 mgGAE/g and 42.97 mgQE/g, respectively, with an IC_{50} value of 8.263 ppm. Docking analysis of 37 test compounds identified 12 compounds with low binding energy, ranging from -7 to -9 kcal/mol, with the NADPH oxidase protein receptor (PDB ID: 2CDU). These compounds include kaempferol-3-rhamnoside, meperidine, apigenin-7-O-glucoside, 2-keto benzothiazole 54, methyl propanoic acid, salicyloylaminotriazole, salicylihalamide A, and gibberellin A7. Our findings suggest that *S. alba* extract holds potential for further exploration as a natural antioxidant source.

Keywords: Antioxidant; In-silico; Metabolomics; *S. alba*

INTRODUCTION

Free radical compounds can be caused by oxidative stress by inducing tissue and cell systems in living things' bodies. They can trigger various degenerative diseases such as cancer, coronary heart disease and premature aging (Neha et al., 2019). The interaction between oxidative stress and the inflammatory process plays an important role, which affects the onset and development of various diseases (Moldogazieva et al., 2018; Sies & Jones, 2020). Oxidation due to free radicals biologically induces the growth of cancer cells. Cancer is one of the leading causes of death worldwide. Despite great efforts to create effective chemotherapy drugs, there are still major problems of toxicity and selectivity. The toxicity of modern chemotherapy and the resistance of cancer cells to anticancer agents make us look for new treatments and methods of preventing this dangerous disease (Tungmunnithum et al., 2018). Defense against free radicals and inhibiting cancer cell growth can be defended by phenol compounds, polyphenols, flavonoids, alkaloids and other compounds that can be obtained from the content of several active compounds found in plants (Behl et al., 2021; Sidoryk et al., 2018). The use of natural ingredients derived from plants (herbs) has been widely used to treat various diseases, due to it has the advantage of being cheaper and having low side effects (Elkordy et al., 2021). Most studies conducted thus far have assessed biological activity by measuring individual compounds separately. However, the bioactivity of a single compound may vary when present in a mixture due to potential synergistic interactions with other components (Vaou et al., 2022). Consequently, reported antioxidant and anticancer compounds may not be solely responsible for the actual antioxidant activity observed in plants. Antioxidants play a crucial role in neutralizing free radicals, thereby protecting cells from oxidative damage and inhibiting cancer cell proliferation. Numerous studies have focused on identifying novel antioxidants to mitigate radical-induced cellular damage and cancer progression (Hassanpour & Doroudi, 2023) Antioxidant and anticancer compounds can be derived from bioactive extracts, secondary metabolites of plants or microbes, and synthetic sources. The

development of antioxidants from natural sources continues to be explored as a promising alternative to synthetic drugs. Flavonoids, a class of polyphenolic secondary metabolites, are widely distributed in plants and food sources, exhibiting various bioactive properties, including antiviral and anti-inflammatory activities (Sidoryk et al., 2018). Phenolic compounds, in particular, demonstrate potent antioxidant and free radical-scavenging properties, along with anti-inflammatory, anti-aging, cardiovascular, and neuroprotective effects.

Indonesia is a tropical country with many potential natural resources based on plants to obtain secondary metabolite compounds as medicinal compounds. One plant species with notable antioxidant potential is Perepat plant *(Sonneratia alba)*, a mangrove species traditionally utilized by the people of Jambi Province for medicinal purposes. Several studies have investigated mangrove plants as sources of bioactive antioxidants. *Sonneratia alba (S. alba)*, a group of mangroves that grow abundantly on the east coast of Sumatra (Sarno et al., 2017), is a type of mangrove with bioactivity capabilities against several tests conducted. *S. alba* has antimicrobial, antioxidant, and cytotoxic activities. Likewise, the acetone and ethanol extracts of *S. alba* leaves showed antioxidant activity (Latief et al., 2018), cytotoxic agent (Latief et al., 2020), and inhibits the growth of gram-negative and gram-positive bacteria (Amilia & Kustiawan, 2024). *S. alba* is a potential plant source of bioactive compounds that can be explored. Ethanol extracts from the bark and leaves of *S. alba* have been reported to contain bioactive compounds with antioxidant activity, particularly phenolic compounds, including 7-hydroxycoumarin (scopoletin). Similar studies employing the DPPH assay have demonstrated that methanol extracts exhibit strong antioxidant activity. These findings indicate that *S. alba* leaves hold promise as a natural antioxidant source (Heriyanti et al., 2024). To date, most studies have primarily utilized crude extracts, such as ethanol, *n*-hexane, and ethyl acetate extracts, in assessing bioactivity. However, fractionation studies are essential to delineate the distribution of bioactive compounds within each fraction of the ethanol extract. Additionally, no comprehensive research has applied a metabolomic approach to examine the multicomponent effects of *S. alba* extracts and fractions. A metabolomic analysis is crucial for identifying the specific compounds responsible for bioactivity, as it enables a holistic evaluation of all metabolites within a sample. This approach integrates in vitro bioassays with molecular docking analyses to establish correlations between metabolite profiles and biological activity (Liu et al., 2022).

Metabolomics utilizes advanced analytical techniques to comprehensively profile metabolites in complex biological samples (Dettmer et al., 2009). Key platforms include nuclear magnetic resonance (NMR) spectroscopy, gas chromatography-mass spectrometry (GC-MS), and liquid chromatography-mass spectrometry (LC-MS) (Alseekh et al., 2021). Oxidative stress plays a crucial role in various pathologies, including neurodegenerative diseases and cancer, making NADPH oxidase—a major source of reactive oxygen species (ROS)—a critical therapeutic target. Molecular docking against NADPH oxidase provides insights into the interactions of bioactive compounds from *S. alba* with oxidative stress-related targets (Mhya et al., 2023). This computational approach elucidates antioxidant mechanisms at the molecular level and aids in identifying lead compounds for drug development. This study aims to profile antioxidant metabolites in *S. alba* leaf extract and assess its potential as a natural antioxidant. By integrating metabolomic analysis with molecular docking, it seeks to enhance understanding of *S. alba*'s antioxidant potential and its therapeutic relevance in oxidative stress-related diseases.

EXPERIMENTAL SECTION

Materials

The materials used in this research were *S. alba* leaves obtained from East Tanjung Jabung Regency Jambi Province Indonesia. Chemicals used in this research: ethanol, 2,2-diphenyl-1-picrylhydrazyl (DPPH), Folin-Ciocalteu, and 3D test compounds, which were saved in pdb format. as well as the structure of the receptor (target protein) NADPH Oxsidase (PDBid: 2CDU) which is stored in pdb form on the web server of each database.

Tools and Instrumentations

The tools used in this research are hardware, namely Lenovo PC IdeaCentre AIO 5i 24IAH7 F0GR006RID Storm Gray (Intel Core i7 12700H, Win11 Home, 16GB DDR4, Intel ARC A370M 4GB GDDR6) and software PyRx, ChemDraw Ultra version 22.0, Chem 3D version 22.0, AutoDockTools, Discovery Studio Visualizer 2021 and UCSF Chimera for the webserver used rscb (Research Collaboratory for Structural Bioinformatics). The instrumentations used: Spectrophotometer UV-Vis (Thermo-Scientific, Singapore) and Liquid Chromatography-Mass Spectra (LC-MS).

Extraction Process

The extraction of bioactive compounds from *S. alba* was conducted following established methodologies, utilizing analytical-grade ethanol (p.a) at five concentration gradients: EP1 (water), EP2 (25% ethanol), EP3 (50% ethanol), EP4 (75% ethanol), and EP5 (100% ethanol). The extraction process employed the maceration technique with a solvent-to-sample ratio of 1:50. Specifically, 100 g of *S. alba* leaf powder was accurately weighed and macerated in 500 mL of ethanol for 24 hr. The resulting macerate was then concentrated using a rotary evaporator, and the obtained extract was subsequently weighed (Silvia et al., 2024).

Determination of Total Phenolic Content and Flavonoids

The phenolic content was determined using the Folin-Ciocalteu reagent, following Taamalli et al, 2014 (Taamalli et al., 2015). An aliquot (0.125 mL) of suitably diluted ethanol extract was mixed with 0.5 mL of deionized water and 0.125 mL of Folin–Ciocalteu reagent (1:1 diluted with deionized water). After 6 minutes, 1.25 mL of 7% sodium carbonate (Na_2CO_3) solution was added to the mixture, followed by 1.0 mL of deionized water to reach a final volume of 3.0 mL. The mixture was incubated at room temperature in the dark for 90 minutes. The absorbance was then measured at 760 nm using a UV–Vis spectrophotometer. Total phenolic content was calculated from a standard curve prepared with gallic acid and expressed as milligrams of gallic acid equivalents per gram of dry matter (mg GAE/g DM). All measurements were performed in triplicate.

Antioxidant Activities

Antioxidant activity was carried out using the DPPH (1,1-diphenyl-2-picrylhydrazyl) method. The DPPH solution was made by dissolving 5 mg of DPPH powder in 50 mL of ethanol. The blank was prepared by added 3 mL of DPPH solution into 1 mL of ethanol. Then, a sample solution was made by dissolved 50 mg of extract in 50 mL of ethanol (p.a). Next, the mixed solution was made by mixing the sample solution in various concentrations (20, 40, 60, 80, 100) ppm, which was added with 3 mL of DPPH solution, then homogenized and left for 30 minutes. Furthermore, it was tested using a UV-Vis Spectrophotometer at a wavelength of 515 nm (Acosta-Otálvaro et al., 2022).

LC-MS/MS Analysis

The crude extract of *S. alba* leaves was analyzed using LC/MS-MS. The results of the LC/MS-MS data analysis obtained a chromatogram in the form of a peak height plot, and the molecular weight of the compounds contained in the extract can be obtained so that you can know the number of compounds contained in each sample. The LC-MS analysis was performed to separate complex mixtures based on differences in the propagation rates of individual components within a specified medium. The separation process involved passing the sample through a chromatographic column, followed by detection and quantification of each component using a mass spectrometry (MS) detector. For the analysis, 10 mg of the sample extract was dissolved in 5 mL of LC-MS/MS-grade methanol. The dissolution process was facilitated using an ultrasonicator for 30 min at room temperature to ensure complete solubilization. Subsequently, the solution was filtered through a 0.2 µm polytetrafluoroethylene (PTFE) membrane filter to remove particulates, and 5 µL of the filtrate was injected into the LC-MS/MS system for analysis. The raw data obtained from the LC-MS/MS analysis were processed using MassLynx V4.1 software. Compound identification was conducted by matching the acquired MS and MS/MS spectra with reference spectra available in online databases. The ChemSpider platform (https://www.chemspider.com/) was utilized to facilitate compound annotation and structural elucidation, ensuring accurate identification of bioactive metabolites (Silvia et al., 2024).

Ligand and Macromolecule Preparation

Ligand preparation is carried out by drawing the 2D structure of the test compound (ligand) using ChemDraw Ultra version 22.0 and then converting it into 3D form using Chem 3D version 22.0 and saving it in pdb format. The test ligands were optimized by minimizing energy using PyRx software with the open Babel feature and then saved in pdbqt format. Furthermore, macromolecular preparation is carried out by downloading the receptor in the https://www.rcsb.org database with the receptor code NADPH Oxsidase (PDBid: 2CDU) Macromolecules are separated from solvents and native ligands or nonstandard residues using the UCSF Chimera application. Native ligands and unnecessary residues are removed by clicking the select feature, then clicking residues and selecting all nonstandard, then selecting the actions feature, clicking atoms/bonds, and then clicking delete. Macromolecular (receptor) files are saved in pdb format. Next, the macromolecules were optimized using AutoDockTools by adding hydrogen ions and Kollman charges and saved in pdbqt file format (Liu et al., 2023; Mhya et al., 2023)

Molecular Docking Validation

Validation of the molecular docking method was carried out using AutoDockTools software. This is done by re-docking the natural ligands of each macromolecule (receptor). The parameter used is Root Mean Square Deviation (RMSD). The results obtained in this process are the grid box parameters and RMSD values. The docking method is valid if it has an RMSD value < 2 Å. The molecular docking process is carried out using Autoodock Tools software. The macromolecule (receptor) and ligand structures that have been optimized separately are stored in one folder. The molecular docking process uses a grid box and energy minimization parameters according to validation results. Grid box parameter settings are carried out using grid box coordinates, which are determined based on the ligand coordinates of the receptor used in the docking validation process. The docking data displayed is in the form of binding affinity values and amino acid residue interactions (Hasan et al., 2023).

Visualization and Analysis of Docking Results

The visualization process is carried out to see the interactions that occur in the docking results between the receptor and the ligand. Visualization of docking results was carried out on the native ligand to find

the right conformation. Conformation docking obtained is the aligned with the native ligand conformation on the crystallographic structure expressed in root-mean-square deviation (RMSD). The RMSD value states that the conformational alignment of the structure is still acceptable with a value of less than 2.5 Å, if it is smaller or closer to the value 0 then the alignment value is getting better using (Chairunisa et al., 2023).

RESULT AND DISCUSSIONS

Total Phenolic, Total Flavonoid, and Antioxidant Activity

Phenolic compound intake may play a fundamental role in antioxidant activity and diabetes management, as it can reduce blood glucose levels, oxidative stress, protein glycation, and other mechanisms (Boukarai et al., 2017). Both, total phenolic and total flavonoid are commonly used to determine the content of phenolic and flavonoid compounds in the sample, which play an essential role as natural antioxidants. **Table 1** results show that the total phenolics and flavonoids in the samples increased with increasing ethanol concentration. Sample EP1 (water) had the lowest phenolic and flavonoid content, 1.007 mg GAE/g and 5.085 mg QE/g, respectively. In contrast, EP5 (100% ethanol) had the highest content, 24.978 mg GAE/g for phenolics and 42.97 mg QE/g for flavonoids. These results are consistent with previous studies showing that ethanol solvents with higher concentrations can extract more phenolic and flavonoid compounds, mainly because of the nature of ethanol, which can dissolve non-polar phenolic compounds more effectively than water. In addition, research by Do et al. 2014 (Do et al., 2014) report that higher ethanol concentrations could extract phenolic compounds more efficiently, supporting the finding that extracts with higher ethanol concentrations have more robust antioxidant activity.

The data in **Table 2** shows the antioxidant activity of various extract samples with various ethanol concentrations, expressed in IC_{50} values (ppm), which indicate the concentration required to inhibit 50% of free radicals. A lower IC_{50} value indicates higher antioxidant activity. Sample EP5 (100% ethanol) had the highest antioxidant activity with an IC_{50} value of 8.263 ppm, followed by EP4 (75% ethanol) with an IC_{50} value of 10.38 ppm, indicating that higher ethanol concentrations tend to produce extracts with more robust antioxidant activity. Ascorbic acid (vitamin C), used as a positive control, had an IC_{50} value of 33.44 ppm, indicating that EP5 and EP4 extracts have higher antioxidant potential than ascorbic acid. These results align with previous research (Do et al., 2014), which reported that extraction with ethanol solvents increased phenolic content, which was positively correlated with antioxidant activity. Overall, the high antioxidant activity at high ethanol concentrations in the extract can be attributed to the ability of ethanol to extract phenolic and flavonoid compounds, which are bioactive compounds with free radical scavenging capacity (Silvia et al., 2024).

Metabolite Profilling

Perepat (*Sonneratia albas*) is a mangrove plant known to contain various bioactive compounds with promising pharmacological potential. In this study, the active compounds in perepat leaves were identified using Liquid Chromatography-Mass Spectrometry (LC-MS), with five different ethanol solvent concentrations: 100% (EP5), 75% (EP4), 50% (EP3), 25% (EP2), and 0% or distilled water (EP1). The LC-MS analysis produced chromatograms showing distinct peaks representing different chemical constituents in each extract. These peaks were analyzed using MassLynx software, and compound identification was performed by referencing databases such as PubChem, ChemSpider, and MassBank. From the interpretation of the LC-MS peaks of the 100% ethanol extract (EP5), a total of 20 compounds were successfully identified (**Figure 1, Table 3**). The 75% ethanol extract (EP4) revealed 15 compounds (**Figure 2, Table 4**), while the 50% ethanol extract (EP3) identified 15 compounds (**Figure 3, Table 5**). The number of detected compounds continued to decrease with lower ethanol concentrations—25% ethanol (EP2) yielded 16 compounds (**Figure 4, Table 6**), and the water extract (EP1) revealed only 19 compounds (**Figure 5, Table 7**). These results indicate that solvent polarity plays a crucial role in the efficiency of extracting bioactive compounds from perepat leaves.

Table 1. Phenolic and flavonoids total

Samples	Phenolics Total (mgGAE/g)	Flavonoids Total (MgQE/g)
EP1 (Water)	1.007	5.085
EP2 (25% Ethanol)	4.467	12.97
EP3 (50% Ethanol)	6.438	23.46
EP4 (75% Ethanol)	12.927	35.73
EP5 (100% Ethanol)	24.978	42.97

Table 2. Antioxidant activities

Samples	Linear regression	IC_{50} (ppm)
Ascorbic Acids	y = 1.8345x – 6.8046	33.44
EP1 (Water)	y = 0.4793x + 22.31	57.77
EP2 (25% Ethanol)	y = 0.5724x + 22.64	40.80
EP3 (50% Ethanol)	y = 0.7621x + 21.782	37.02
EP4 (75% Ethanol)	y = 0.531x + 44.48	10.38
EP5 (100% Ethanol)	y = 0.724 + 28.678	8.263

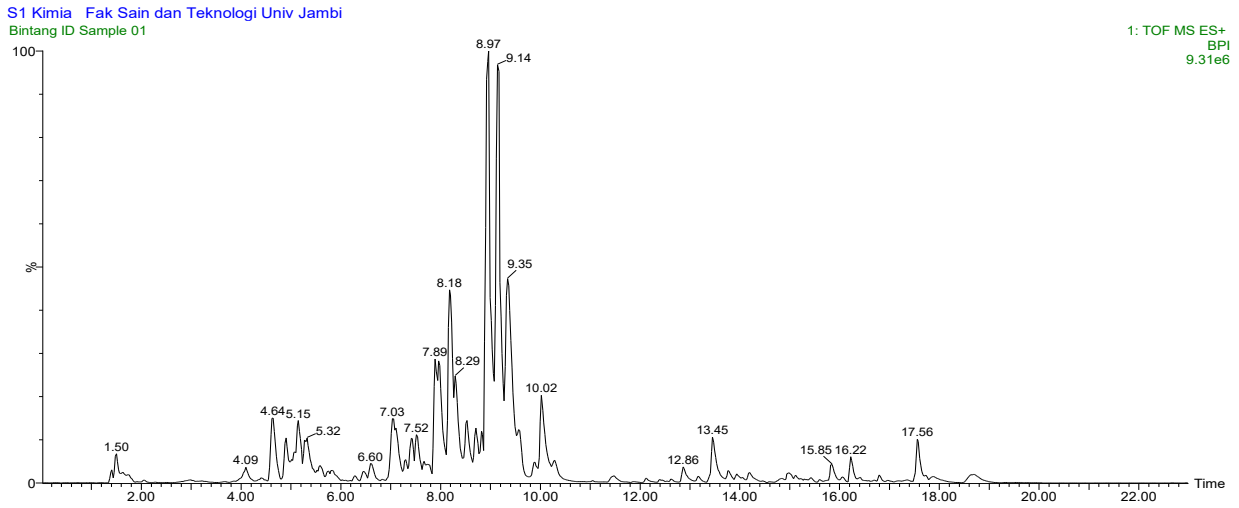

Figure 1. LC-MS chromatogram of EP5

Table 3. Putative compounds profile in EP5

No	RT	Putative Compounds	Formulas	Mass	MW (g/mol)
1	1.50	4*H*-cyclopenta[def]phenanthrene-4-one	$C_{15}H_8O$	204.06	204.23
2	4.09	Meperidine	$C_{15}H_{21}NO_2$	247.16	247.34
3	4.64	Scolymoside	$C_{27}H_{30}O_{15}$	594.16	594.52
4	4.90	2'-Hydroxygenistein-7-O-glucoside	$C_{21}H_{20}O_{11}$	448.10	448.38
5	5.15	Kaempferol 3-gluco-xyloside	$C_{26}H_{28}O_{15}$	580.14	580.50
6	5.32	Kaempferol-3-Rhamnoside	$C_{21}H_{20}O_{10}$	432.11	432.38
7	6.60	2,4-Diamino-6-morpholino-s-triazine	$C_7H_{12}N_6O$	196.11	196.21
8	7.03	3-(4,6-dimorpholino-1,3,5-triazin-2-yl)-1,2,3,4,5,6-hexahydro-8*H*-1,5-methanopyridol[1,2-a] [1,5] diazocin-8-one	$C_{22}H_{29}N_7O_3$	439.23	439.52
9	7.52	4-[4-(Benzyloxy)-2-methylbenzoyl]-5-(4-ethoxyphenyl)-3-hydroxy-1-[3-(4-morpholinyl)propyl]-1,5-dihydro-2H-pyrrol-2-one	$C_{34}H_{38}N_2O_6$	570.27	570.69
10	7.89	N-[3-(4-{[(5-Isopropyl-1,2-oxazol-3-yl)carbamoyl]amino}-3-methylphenyl)-1H-pyrazol-5-yl]-4-[(4-methyl-1-piperazinyl)methyl]benzamide	$C_{30}H_{36}N_8O_3$	556.29	556.67
11	8.18	Linetastine	$C_{35}H_{40}N_2O_6$	584.29	584.71
12	8.29	L-Histidyl-1-(2-hydroxy-5-nitrobenzyl)-L-tryptophyl-L-lysine	$C_{30}H_{36}N_8O_7$	620.27	620.67
13	8.97	5-Isothiocyanatoindane	$C_{24}H_{42}N_8O_8$	570.31	570.65
14	9.14	N-[3-(4-{[(5-Tert-Butyl-1,2-Oxazol-3-Yl)carbamoyl]amino}-3-Methylphenyl)-1h-Pyrazol-5-Yl]-4-[(4-Methylpiperazin-1-Yl)methyl]benzamide	$C_{31}H_{38}N_8O_3$	570.31	570.70

15	9.35	1-{6-(3,4-Dihydro-2(1H)-isoquinolinyl)-2-[4-(2-methyl-2-propanyl)phenyl]-4-pyrimidinyl}-3-(1-methyl-1H-indol-3-yl)-2-piperazinone	$C_{36}H_{38}N_6O$	570.31	570.74
16	10.02	2-[(2-Methoxy-4-{[4-(4-methyl-1-piperazinyl)-1-piperidinyl]carbonyl}phenyl)amino]-5,11-dimethyl-5,11-dihydro-6H-pyrimido[4,5-b][1,4]benzodiazepin-6-on	$C_{31}H_{38}N_8O_3$	570.31	570.70
17	12.86	N-[2-Amino-6-(butylamino)-3-hydroxy-5-methyl-6-oxohexyl]-N-isopropyl-4-methoxy-3-(3-methoxypropoxy)benzamide	$C_{26}H_{45}N_3O_6$	495.33	495.66
18	13.45	4-[({4-[3-Ethyl-7-(4-morpholinyl)-3H-[1,2,3]triazolo[4,5-d]pyrimidin-5-yl]phenyl}carbamoyl)amino]-N-[2-(2-pyridinyl)ethyl]benzamide	$C_{31}H_{32}N_{10}O_3$	592.27	592.66
19	15.85	Ethyl N-[(2-{[(4-carbamoylphenyl)amino]methyl}-1-methyl-1H-benzimidazol-5-yl)carbonyl]-N-2-pyridinyl-β-alaninate	$C_{27}H_{28}N_6O_4$	500.22	500.56
20	16.22	N-[3-(4-{[(5-Isopropyl-1,2-oxazol-3-yl)carbamoyl]amino}-3-methylphenyl)-1H-pyrazol-5-yl]-4-[(4-methyl-1-piperazinyl)methyl]benzamide	$C_{30}H_{36}N_8O_3$	556.29	556.67

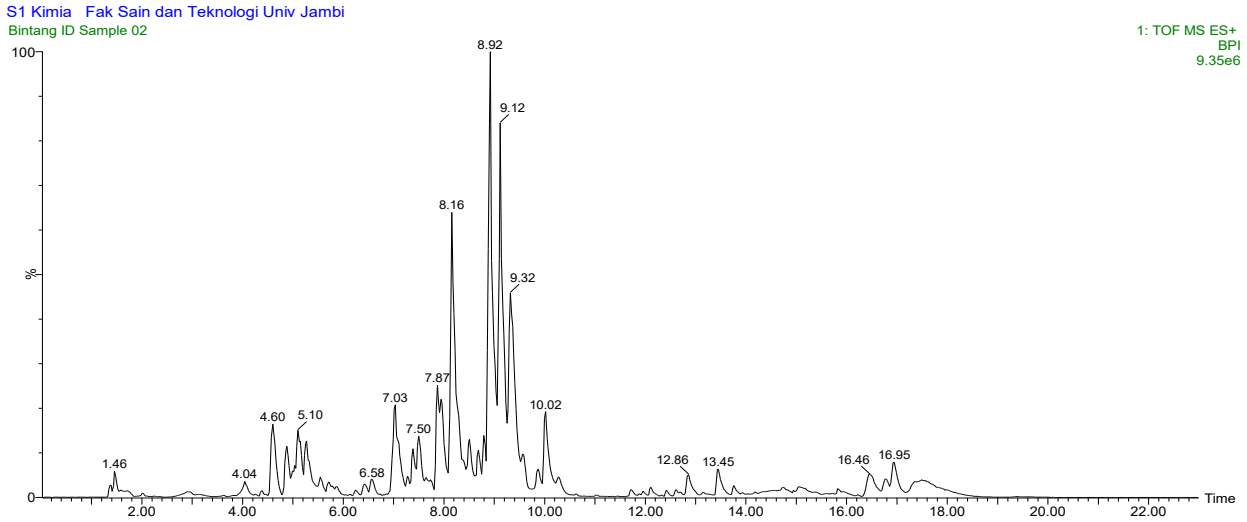

Figure 2. LC-MS chromatogram of EP4

Table 4. Putative compounds profile in EP4

No	RT	Putative Compounds	Formulas	Mass	MW (g/mol)
1	1.46	6-[2-(2-Ethyl-4-methyl-1H-imidazol-1-yl)ethyl]-1,3,5-triazin-2,4-diamin	$C_{11}H_{17}N_7$	247.15	247.31
2	4.04	Biurea, 1,6-dimethyl-1,6-dinitroso-	$C_4H_8N_6O_4$	204.06	204.15
3	4.60	1,8-Dihydroxy-6-methoxy-9-oxo-9H-xanthen-2-yl 2-O-(6-deoxy-α-L-mannopyranosyl)-β-D-xylopyranoside	$C_{25}H_{28}O_{14}$	552.15	552.49
4	5.10	Carlinoside	$C_{26}H_{28}O_{15}$	580.14	580.50
5	5.27	7-(4-Aminobenzyl)-7H-pyrrolo[3,2-f]quinazoline-1,3-diamine	$C_{17}H_{16}N_6$	432.10	432.35
6	6.58	2,4-Diamino-6-morpholino-s-triazine	$C_7H_{12}N_6O$	196.11	196.21

7	7.03	11-[4,6-Di(4-morpholinyl)-1,3,5-triazin-2-yl]-7,11-diazatricyclo[7.3.1.0~2,7~]trideca-2,4-dien-6-one	$C_{22}H_{29}N_7O_3$	439.23	439.52
8	7.50	4-[4-(Benzyloxy)-2-methylbenzoyl]-5-(4-ethoxyphenyl)-3-hydroxy-1-[3-(4-morpholinyl)propyl]-1,5-dihydro-2H-pyrrol-2-one	$C_{34}H_{38}N_2O_6$	570.27	570.69
9	7.87	4-[(4-Methylpiperazin-1-Yl)methyl]-N-{3-[3-Methyl-4-({[5-(Propan-2-Yl)-1,2-Oxazol-3-Yl]carbamoyl}amino)phenyl]-1h-Pyrazol-5-Yl}benzamide	$C_{30}H_{36}N_8O_3$	556.29	556.67
10	8.16	2-Methyl-2-propanyl {(2S,3S)-1-[(3S)-7-[2-(hydroxyamino)-2-oxoethoxy]-3-[(4-methoxyphenyl)carbamoyl]-3,4-dihydro-2(1H)-isoquinolinyl]-3-methyl-1-oxo-2-pentanyl}carbamate	$C_{30}H_{40}N_4O_8$	584.28	584.67
11	8.79	N-Methyl-D-phenylalanyl-N-[5-carbamimidamido-1-(1-methyl-1H-benzimidazol-2-yl)-1-oxo-2-pentanyl]-L-prolinamide	$C_{29}H_{38}N_8O_3$	546.31	546.68
12	9.12	2-[(2-Methoxy-4-{[4-(4-methyl-1-piperazinyl)-1-piperidinyl]carbonyl}phenyl)amino]-5,11-dimethyl-5,11-dihydro-6H-pyrimido[4,5-b][1,4]benzodiazepin-6-on	$C_{31}H_{38}N_8O_3$	570.31	570.70
13	9.32	5-[4-(Benzyloxy)phenyl]-4-(4-butoxybenzoyl)-1-[3-(diethylamino)propyl]-3-hydroxy-1,5-dihydro-2H-pyrrol-2-one	$C_{35}H_{42}N_2O_5$	570.31	570.73
14	12.86	2-{(2R,3R,6S)-2-{[(1R,2S,3S,4R,6S)-4,6-Diamino-3-{[3-deoxy-4-C-methyl-3-(methylamino)-L-arabinopyranosyl]oxy}-2-hydroxycyclohexyl]oxy}-6-[(1R)-1-(methylamino)ethyl]tetrahydro-2H-pyran-3-yl}guanidine	$C_{22}H_{45}N_7O_7$	519.34	519.64
15	13.45	N-Cyclopentyl-N-[2-(dimethylamino)ethyl]-2-(5-{[isopropyl(methyl)amino]methyl}-1-tetrazolidinyl)acetamide	$C_{17}H_{37}N_7O$	355.31	355.53

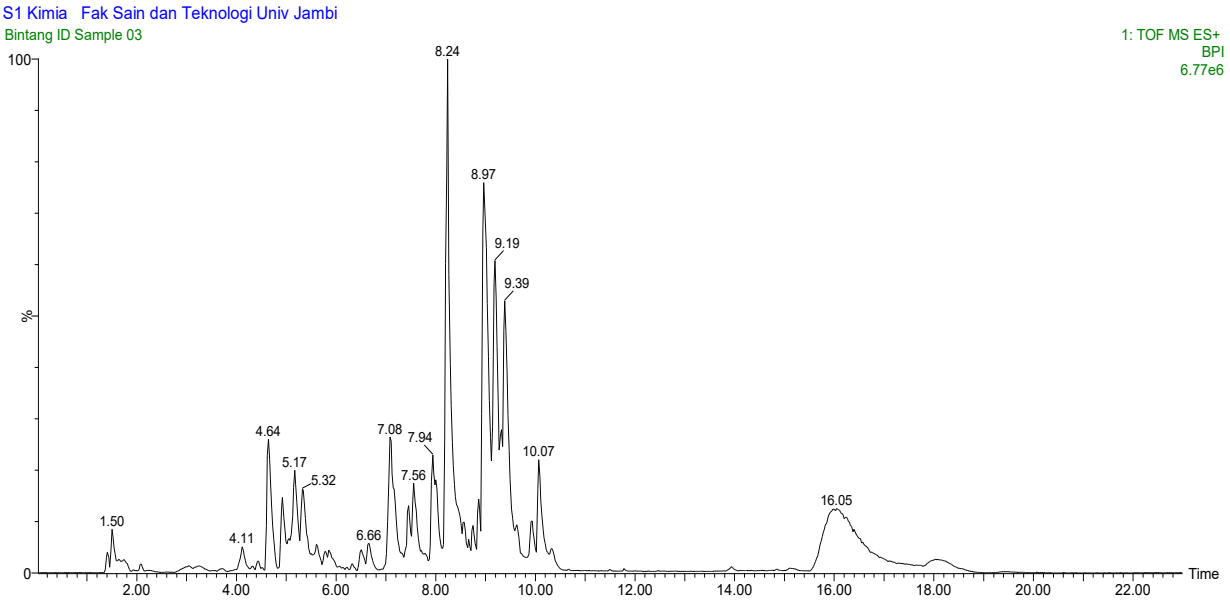

Figure 3. LC-MS chromatogram of EP3

Table 5. Putative compounds profile in EP3

No	RT	Putative Compounds	Formula	Mass	MW (g/mol)
1	1.50	Salicyloylaminotriazole	$C_9H_8N_4O_2$	204.06	204.19
2	4.11	Meperidine	$C_{15}H_{21}NO_2$	247.16	247.34
3	4.64	Kaempferol-3-O-rutinoside	$C_{27}H_{30}O_{15}$	594.16	594.52
4	4.92	Quercitrin	$C_{21}H_{20}O_{11}$	448.10	448.38
5	5.17	Quercetin 3-[rhamnosyl-(1->2)-alpha-L-arabinopyranoside]	$C_{26}H_{28}O_{15}$	580.14	580.50
6	5.32	Apigenin-7-O-glucoside	$C_{21}H_{20}O_{10}$	432.11	432.38
7	6.66	Isobutyl furfurylacetate	$C_{11}H_{16}O_3$	196.11	196.25
8	7.08	(S)-2-(3-(1-((4-Isopropylbenzyloxy)carbonyl)piperidin-3-yl)phenoxy)-2-methylpropanoic acid	$C_{26}H_{33}NO_5$	439.24	439.55
9	7.56	Dipiperamide A	$C_{34}H_{38}N_2O_6$	570.27	570.69
10	7.94	Omadacycline	$C_{29}H_{40}N_4O_7$	556.29	556.66
11	8.24	2-[[1-[(1-Carboxy-2-phenylethyl)amino]-4-methyl-1-oxopentan-2-yl]amino]-4-[2-(phenylmethoxycarbonylamino) propanoylamino]butanoic acid	$C_{30}H_{40}N_4O_8$	584.28	584.67
12	8.86	2-ketobenzothiazole 54	$C_{29}H_{38}N_8O_3$	546.31	546.68
13	8.97	N-{2-(2-Methyl-2-propanyl)-6-[4-(4-phenoxyphenyl)-1-piperazinyl]-4-pyrimidinyl}-N′-phenyl-1,4-benzenediamine	$C_{36}H_{38}N_6O$	570.31	570.74
14	9.19	Hydroxyethylene dipeptide isostere 8	$C_{35}H_{42}N_2O_5$	570.31	570.73
15	9.39	Pyrazolo[3,4-d]pyrimidine 6	$C_{31}H_{38}N_8O_3$	570.31	570.70

Tabel 6. Putative compounds profile in EP2

No	RT	Putative Compounds	Formulas	Mass	MW (g/mol)
1	1.39	(3-Aminopropyl)carbamodithioic acid	$C_4H_{10}N_2S_2$	150.03	150.26
2	1.48	3-O-Ethylascorbic acid	$C_8H_{12}O_6$	204.06	204.18
3	4.09	Meperidine	$C_{15}H_{21}NO_2$	247.16	247.34
4	4.64	Nictoflorin	$C_{27}H_{30}O_{15}$	594.16	594.52
5	5.17	3,5-Dicaffeoyl-4-succinoylquinic acid	$C_{29}H_{28}O_{15}$	616.14	616.53
6	5.32	Genistin	$C_{21}H_{20}O_{10}$	432.11	432.38
7	5.85	Ibuprofen	$C_{13}H_{18}O_2$	206.13	206.29
8	6.48	p-Hexyloxybenzoic Acid	$C_{13}H_{18}O_3$	222.13	222.28
9	7.08	Salicylihalamide A	$C_{26}H_{33}NO_5$	439.24	439.55
10	7.56	3,3-Bis-(4-ethyl-phenyl)-2-(4-methoxy-6-methyl-pyrimidin-2-yloxy)-3-[2-(4-methoxy-phenyl	$C_{34}H_{38}N_2O_6$	570.27	570.69
11	7.94	Omadacycline	$C_{29}H_{40}N_4O_7$	556.29	556.66
12	8.22	Linetastine	$C_{35}H_{40}N_2O_6$	584.29	584.71
13	8.97	Pyrazolo[3,4-d]pyrimidine 6	$C_{31}H_{38}N_8O_3$	570.31	570.70
14	9.19	Hydroxyethylene dipeptide isostere 8	$C_{35}H_{42}N_2O_5$	570.31	570.73
15	10.07	5-[4-(Benzyloxy)phenyl]-4-(4-butoxybenzoyl)-1-[3-(diethylamino)propyl]-3-hydroxy-1,5-dihydro-2H-pyrrol-2-one	$C_{35}H_{42}N_2O_5$	570.31	570.73
16	14.31	Methyloctadecylamine	$C_{19}H_{41}N$	283.32	283.54

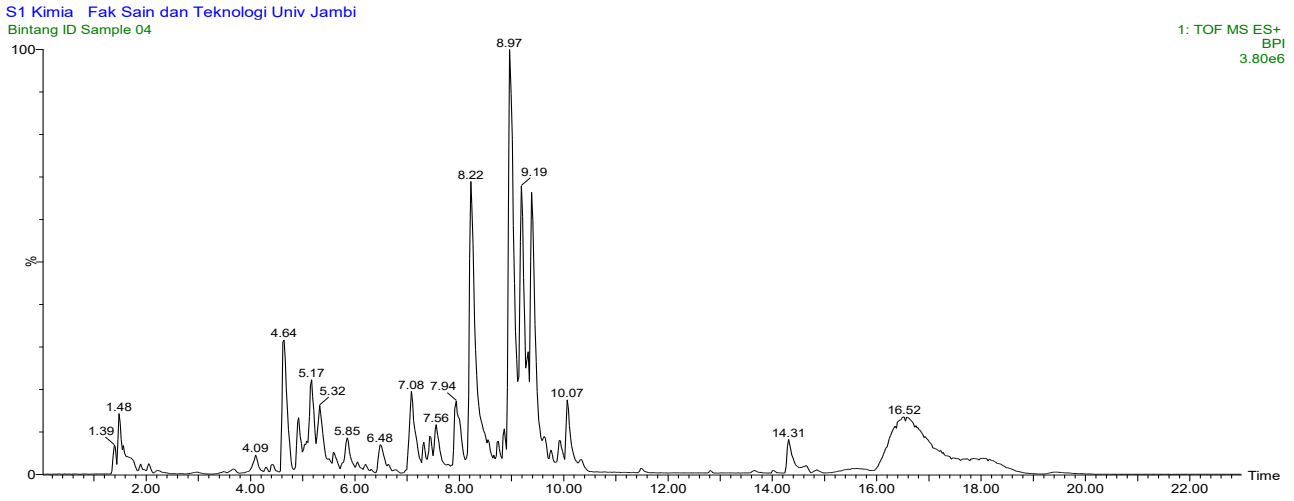

Figure 4. LC Chromatogram EP2

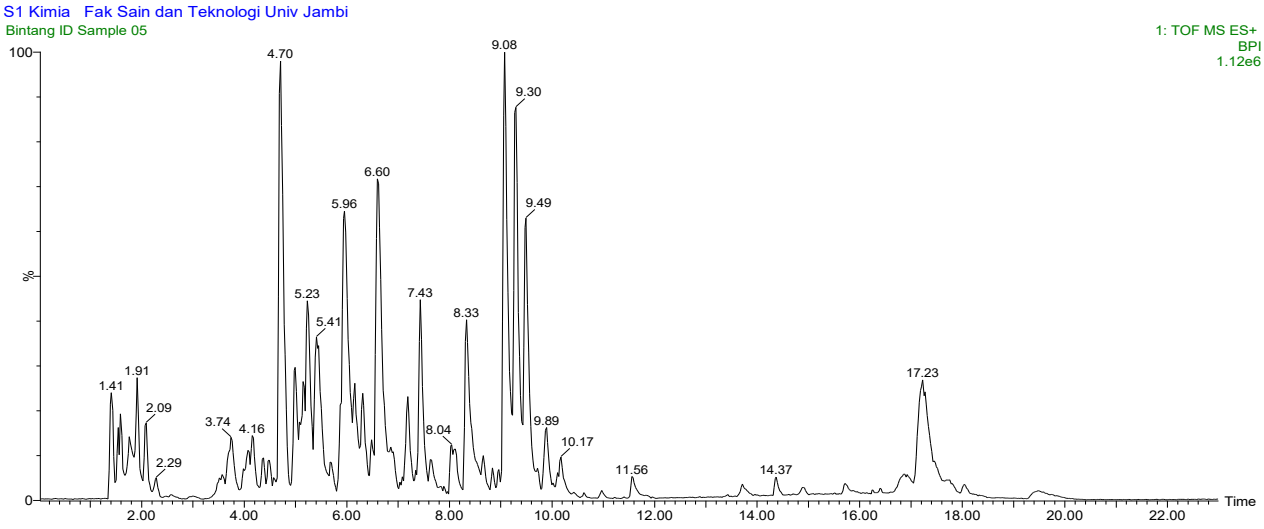

Figure 5. LC-MS Chromatogram EP1

Tabel 7. Putative compounds profile in EP1

No	RT	Putative Compounds	Formulas	Mass	MW (g/mol)
1	1.41	2-Aminobenzothiazole	$C_7H_6N_2S$	150.03	150.20
2	2.09	Homocycloleucine	$C_7H_{13}NO_2$	143.09	143.19
3	3.74	Pantothenic acid	$C_9H_{17}NO_5$	219.11	219.24
4	4.16	Meperidine	$C_{15}H_{21}NO_2$	247.16	247.34
5	4.70	Nictoflorin	$C_{27}H_{30}O_{15}$	594.16	594.52
6	5.23	Carlinoside	$C_{26}H_{28}O_{15}$	580.14	580.50
7	5.41	Apigenin-7-O-glucoside	$C_{21}H_{20}O_{10}$	432.11	432.38
8	5.96	Ibuprofen	$C_{13}H_{18}O_2$	206.13	206.29
9	6.60	2-Hydroxyibuprofen	$C_{13}H_{18}O_3$	222.13	222.28
10	7.19	1-(1-(2-ethoxyethyl)-3-methyl-7-((4-methylpyridin-2-yl)amino)-1H-pyrazolo[4,3-d]pyrimidin-5-yl)piperidine-4-carboxylic acid	$C_{22}H_{29}N_7O_3$	439.23	439.52
11	7.43	Gibberellin A7	$C_{19}H_{22}O_5$	330.15	330.38
12	8.04	Omadacycline	$C_{29}H_{40}N_4O_7$	556.29	556.66
13	8.33	N-(3-((2-(4-amino-1,2,5-oxadiazol-3-yl)-1-ethyl-1H-imidazo[4,5-c]pyridin-6-yl)oxy)phenyl)-4-(2-(diisopropylamino)ethoxy)benzamide	$C_{31}H_{36}N_8O_4$	584.29	584.68

14	9.08; 9.30; 9.49	4-(1-(adamantan-1-ylmethyl)-3,3-bis((1-methyl-1H-imidazol-5-yl)methyl)-2-oxoindolin-6-yl)benzonitrile	$C_{36}H_{38}N_6O$	570.31	570.74
15	9.89	Adamantanecarboxylic acid	$C_{11}H_{16}O_2$	180.12	180.25
16	10.17	Hydroxyethylene dipeptide isostere 8	$C_{35}H_{42}N_2O_5$	570.31	570.73
17	11.56	1-hexadecanal	$C_{16}H_{32}O$	240.25	240.43
18	14.37	Methyloctadecylamine	$C_{19}H_{41}N$	283.32	283.54
19	17.23	4-(((5S,8S,11S,14S,17S,18S)-8-(aminomethyl)-11-isobutyl-5-isopropyl-18-methyl-4,7,13,16-tetraoxo-14-propyl-3,6,9,12,15-pentaazaicosan-17-yl)carbamoyl)pyridine 1-oxide	$C_{33}H_{58}N_8O_6$	662.45	662.88

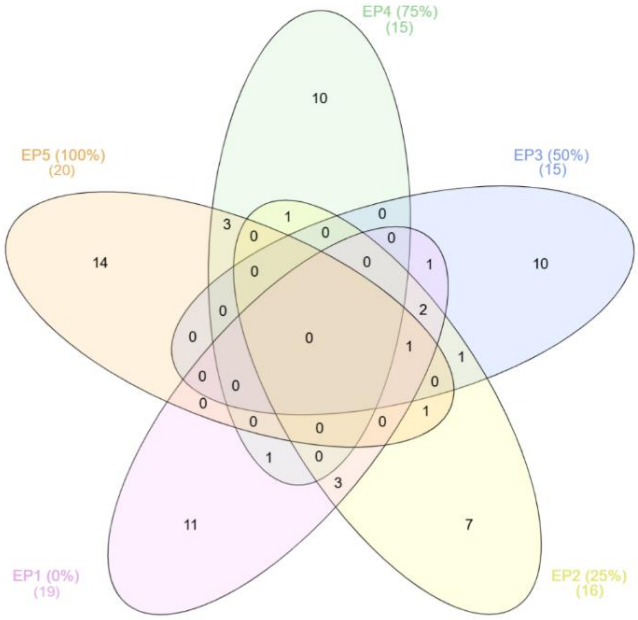

Figure 6. A Venn diagram of five different fractions

Table 8. Venn diagram results of the same active compound from five different fractions

Samples	Total	Active Compounds	Compound Codes
EP1; EP2; EP3; EP5	1	Meperidine	C1
EP1; EP2; EP3	2	Hydroxyethylene dipeptide isostere 8; Omadacycline	C2; C3
EP4; EP5	3	4-[4-(Benzyloxy)-2-methylbenzoyl]-5-(4-ethoxyphenyl)-3-hydroxy-1-[3-(4-morpholinyl)propyl]-1,5-dihydro-2H-pyrrol-2-one; 2-[(2-Methoxy-4-{[4-(4-methyl-1-piperazinyl)-1-piperidinyl]carbonyl}phenyl)amino]-5,11-dimethyl-5,11-dihydro-6H-pyrimido[4,5-b][1,4]benzodiazepin-6-on; 2,4-Diamino-6-morpholino-s-triazine	C4; C5; C6
EP2; EP5	1	Linetastine	C7
EP2; EP4	1	5-[4-(Benzyloxy)phenyl]-4-(4-butoxybenzoyl)-1-[3-(diethylamino)propyl]-3-hydroxy-1,5-dihydro-2H-pyrrol-2-one	C8
EP1; EP4	1	Carlinoside	C9
EP2; EP3	1	Pyrazolo[3,4-d]pyrimidine 6	C10
EP1; EP3	1	Apigenin-7-O-glucoside	C11
EP1; EP2	3	Nictoflorin; Ibuprofen; Methyloctadecylamine	C12; C13; C14

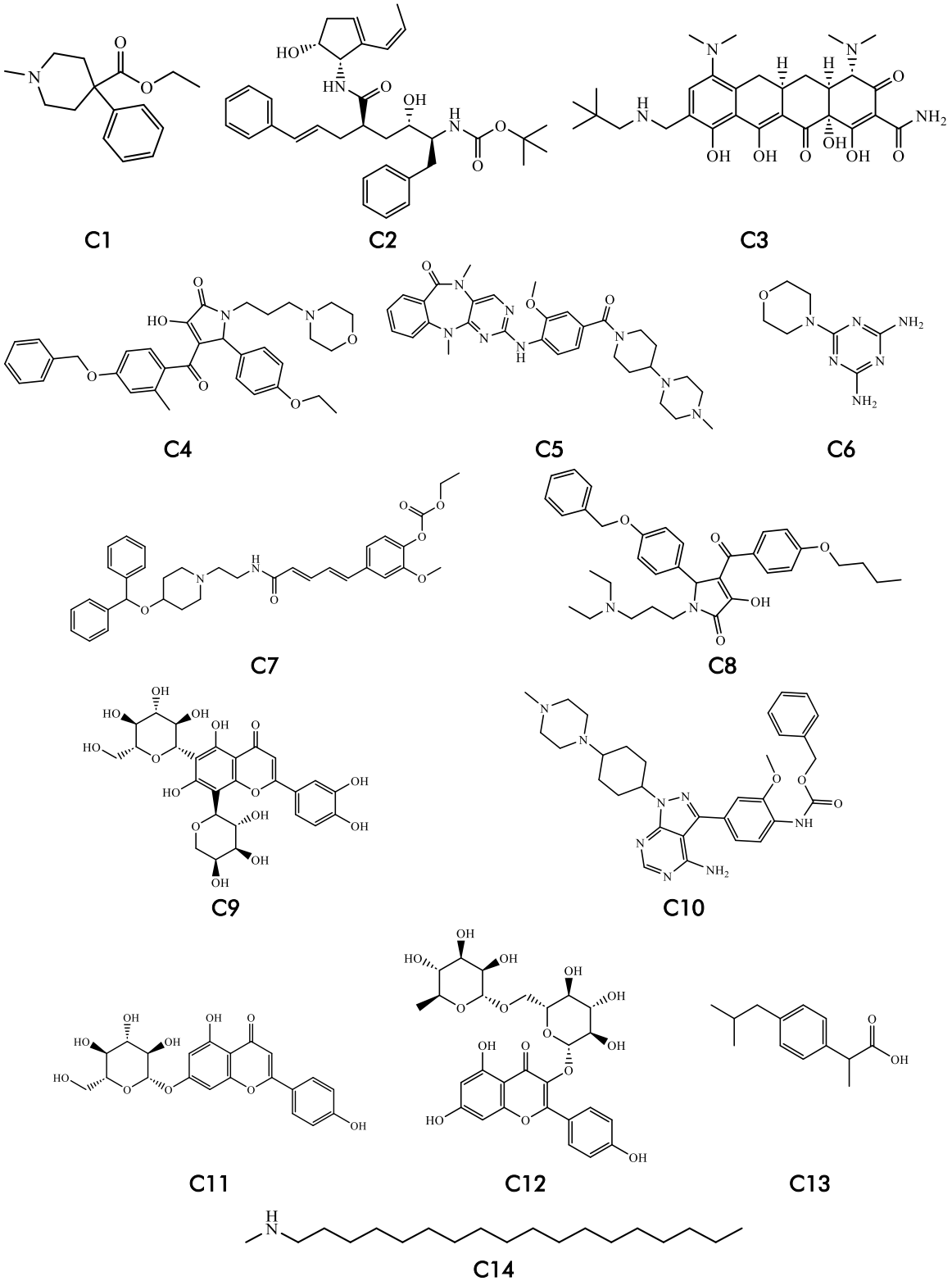

Figure 7. Structures of 14 active compounds from five different fractions

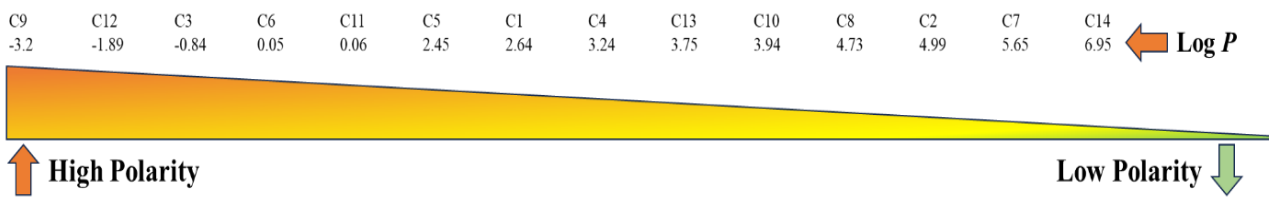

Figure 8. Different polarity of 14 compounds from five different fractions

LC-MS analysis of ethanol extracts from *S. alba* leaves revealed that ethanol concentration influences the composition of extracted compounds. The 100% ethanol extract contained 20 identifiable compounds, while EP4 and EP3 each yielded 15, and EP2 and EP1 contained 16 and 19, respectively. Variations in ethanol concentration resulted in the loss or formation of compounds, as different solvent concentrations extract compounds based on polarity. Higher ethanol concentrations favor nonpolar compounds, whereas lower concentrations extract more polar compounds, following the "like dissolves like" principle. A total of 87 active compounds were identified across all samples, with 14 common to all five extracts (**Table 8**) The Venn diagram illustrates the shared active compounds among the analyzed fractions (**Figure 6**).

The 14 compounds (**Figure 7**) were determined based on the log P value. Log p (partition coefficient) shows the solubility ratio of a substance in octanol and water. The interpretation of the log P value is: Log P > 0 indicates non-polar compounds; Log P < 0 indicates pola r compounds; and Log P = 0 indicates semi-polar compounds. The results of the analysis on 14 compounds can be seen in the **Figure 8**. Where of the 14 compounds, compound C9 (Carlinoside) is the most polar and compound C14 (Methyloctadecylamine) is the most non-polar.

Molecular Docking

The LC-MS/MS analysis identified 69 putative compounds, which were subsequently evaluated for their physicochemical properties using the SwissADME platform (http://www.swissadme.ch/). This assessment was based on **Lipinski's Rule of Five**, a widely accepted criterion for screening drug-like compounds in early-stage drug discovery. According to Lipinski's rules, a compound is considered to have favorable oral bioavailability if it meets the following parameters: molecular weight ≤ 500 Da, hydrogen bond donors ≤ 5, hydrogen bond acceptors ≤ 10, and Log P ≤ 4.15 (29). Among the 69 compounds analyzed, 37 satisfied Lipinski's criteria, indicating their potential as drug candidates, while the remaining compounds deviated from these parameters (**Supplementary Table 1**). This aligns with previous studies, where secondary metabolites from natural products often exhibit drug-like properties but may also violate certain Lipinski criteria due to their structural complexity and high molecular weight (Ivanović et al., 2020; Santana et al., 2021).

Subsequently, the 37 compounds that met Lipinski's rules were subjected to **ADMET (Absorption, Distribution, Metabolism, Excretion, and Toxicity) profiling** using the **pkCSM pharmacokinetics** platform (*https://biosig.lab.uq.edu.au/pkcsm/*). ADMET analysis is crucial in evaluating a compound's pharmacokinetic behavior and safety profile, which are key determinants in drug development. The results of the ADMET analysis, which provide insights into the drug-likeness and potential toxicity of these compounds, are summarized in **supplementary Table 2**. Comparative studies have demonstrated the importance of integrating **Lipinski's rules with ADMET predictions** to refine compound selection in drug discovery. Lipinski's rules provide an initial screening framework, ADMET properties must be considered to ensure compounds exhibit optimal pharmacokinetic and safety characteristics (Abdul-Hammed et al., 2021). Therefore, the integration of these computational approaches enhances the identification of promising bioactive compounds from *S. alba* for further development as therapeutic agents.

From **supplementary Table 2**, the Caco-2 permeability value indicates the absorption of a compound or drug in the intestine. The Caco-2 prediction value > 0.90 means that the compound or drug will likely be well absorbed through the intestinal wall when consumed orally. In intestinal absorption, if the value is <30%, it indicates that the absorption of the drug compound is not good. The log Kp value of > -2.5 indicates good skin permeability, where the drug compound is likely to penetrate the layers of the skin easily.

On the other hand, the VDess (Volume of Distribution at Steady State) value is a parameter used to indicate the distribution of drugs in the body, with parameters including: low < 0.71 L/kg; medium 0.71 - 2.81 L/kg, and high > 2.81 L/kg. A low VDess value indicates that the drug will be concentrated in the blood plasma; a high VDess value indicates that the drug can be widely distributed to tissues and organs. The BBB (Blood-Brain Barrier) v alue is the ability of a compound or drug to penetrate the blood-brain barrier, where log BB> 0.3 indicates good penetration and log BB <-1 indicates poor penetration. The CNS (Confident Number System) value is similar to the BBB value, with the condition that the log PS value> -2 indicates good permeability and log PS <-3 indicates poor permeability. Compounds with a CNS permeability value of less than 2 are generally considered to exhibit good permeability across the blood-brain barrier (BBB). Total clearance (CLtotal) represents the rate at which a compound or drug is eliminated from the body, primarily through excretory organs such as the liver and kidneys. A high clearance value indicates rapid elimination, whereas a low clearance value suggests prolonged retention within the body. Based on the ADMET profile analysis of the 37 identified compounds, 18 compounds exhibited favorable Caco-2 permeability, indicating their potential for efficient intestinal absorption. The distribution profiles of all compounds demonstrated promising results, with the average volume of distribution at steady state (VDss) being relatively low, suggesting that these compounds are

more likely to remain concentrated in the bloodstream rather than being extensively distributed into tissues.

Furthermore, seven compounds—4H-cyclopenta[def]phenanthrene-4-one, meperidine, ibuprofen, 2-amino benzothiazole, adamantane carboxylic acid, 1-hexadecanal, and methyl octadecylamine—exhibited high BBB permeability, indicating their potential to cross the blood-brain barrier effectively. Additionally, six compounds: 4H-cyclopenta[def]phenanthrene-4-one, meperidine, ibuprofen, adamantane carboxylic acid, 1-hexadecanal, and methyl octadecylamine—demonstrated high CNS permeability, making them strong candidates for central nervous system-related applications. This analysis suggests that these compounds may have significant pharmacological potential, particularly for therapeutic applications targeting the CNS. Further in vitro and in vivo evaluations are necessary to confirm their bioavailability and therapeutic efficacy.

The Receptor Analysis

The receptor used is the NADPH Oxidase enzyme (PDBid: 2CDU). The receptor was obtained from the RCSB PDB website (https://www.rcsb.org/). Receptor analysis was carried out using the PDBsum website (https://www.ebi.ac.uk/thornton-srv/databases/pdbsum/), which aims to see whether or not the receptor will be used well. From the results of the analysis using PDBsum, a Ramachandan plot will be obtained. Ramacahandan plot is a two-dimensional plot that illustrates the amino acid residues in the protein structure, as well as the visualization of the three-dimensional coordinates of the protein that have been realized through experiments into internal coordinates consisting of dihedral angles (Φ) as the x-axis and angles (Ψ) as the y-axis of the amino acid residues of the protein structure (Joosten & Lütteke, 2017). These two angles describe the rotation around certain bonds in the amino acid chains that make up the protein. where the shape or structure of the protein, is strongly influenced by steric hindrance, which is the physical restriction that occurs when parts of the protein collide or get too close to each other. Accordingly by plotting the protein structure in a Ramachandan plot, it can be determined whether the structure is valid and appropriate, and has a theoretically stable structure (Pražnikar et al., 2019).

The results of the Ramachandan plot analysis show that in quadrant I there are 90.3% amino acid residues, quadrant II 9.3%, quadrant III 0.4% and in quadrant IV 0.0% which means that the receptor has good stability (**Figure 9**). The Ramachandran plot consists of four quadrants and four regions. The four regions are most favored regions (quadran I), additionally allowed regions (quadran II), generously allowed regions (quadran III), and disallowed regions (quadran IV). From the plot, the structural quality of a protein can be determined by looking at the plot of non-glycine residues located in the disallowed region. Glycine has no side chains so its Φ and Ψ angles are in the four quadrants of the Ramachandran plot. A protein structure can be said to be good if it has the number of residue plots in the most favored region of more than 90% and the R-factor is not more than 20%.

12 Compounds That Possess Low Binding Energy

Molecular docking validation was performed using Autodock Tools software with the principle of re-docking with receptors and native ligands. The native ligand used in this validation is Adenosine diphosphate. This validation aims to determine the grid box size and appropriate coordinates to obtain an RMSD value of ≤ 2 Å. The docking process is valid if the RMSD value is ≤ 2 Å. From the redocking process, the validation results include: grid box x, y, and z are 34, 34, and 36 with coordinates x, y, and z are 18.508; -6.355; and -1.809. Has a distance of 0.375 Å and an RMSD value of 1.17 Å.

Docking analysis of 37 test compounds identified eight with strong interactions with the NADPH oxidase receptor (PDB ID: 2CDU) (**Figure 10**): kaempferol-3-rhamnoside, meperidine, apigenin-7-O-glucoside, 2-ketobenzothiazole 54, methylpropanoic acid, salicyloylaminotriazole, salicylihalamide A, and gibberellin A7 (**Figure 11**). The evaluation parameters included free energy, inhibition constant, hydrogen bonds, and amino acid residue similarity to the native ligand. The native ligand exhibited a free energy of -7.14 kcal/mol, an inhibition constant of 5.84 μM, six hydrogen bonds, and interactions with 12 amino acid residues (**Supplementary Table 3**). Lower free energy values indicate stronger ligand-receptor binding stability, while smaller inhibition constants correlate with enhanced docking performance (Thafar et al., 2019).

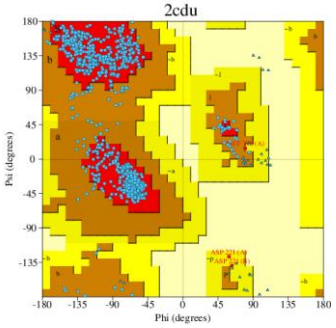

Figure 9. Plot Ramachandan NADPH oxsidase (kode PDB: 2CDU)

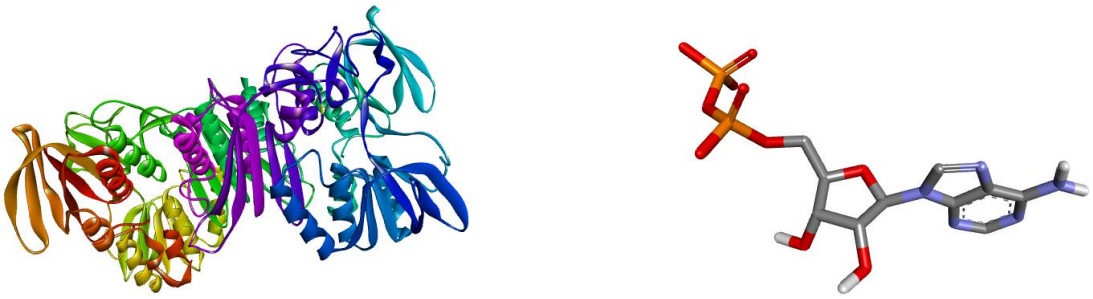

A B

Figure 10. Molecular structure (**a**) Reseptor NADPH oxidase (PBDid: 2CDU) dan (**b**) Native ligan adenosin diphosphate

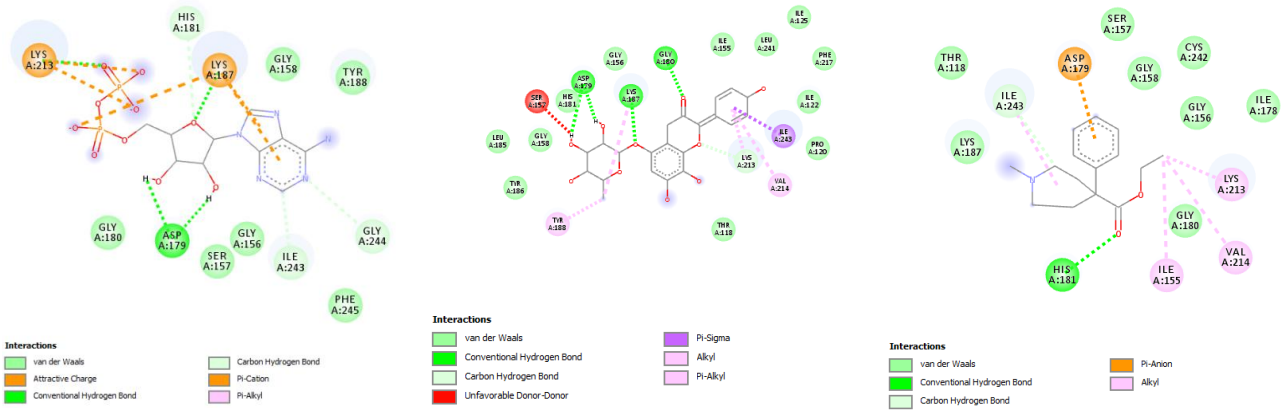

Figure 11. 2D visualization of molecular docking results

While the test ligands, namely kampferol-3-rhamnoside, meperidine, apigenin-7-O-glucoside, 2-ketobenzothiazole 54, methylpropanoic acid, salicyloylaminotriazole, salicylihalamide A and gibberellin A7 have free energy values and inhibition constants respectively: -7.11 kcal/mol; -7.32 kcal/mol; -7.57 kcal/mol; -7.47 kcal/mol; -8.12 kcal/mol; -7.10 kcal/mol; -7.67 kcal/mol, -8.14 kcal/mol and 6.10 μM, 4.30 μM, 2.81 μM, 3.35 μM, 1.12 μM, 6.27 μM, 2.41 μM and 1.09 μM with an average number of amino acid residues of around 17 and 3 hydrogen bonds. The hydrogen bond in the docking results shows the binding strength between the protein receptor and the test ligand, where the greater the number of hydrogen bonds, the more stable the interaction that occurs between the receptor and ligand. At the same time, the amino acid residue shows the binding part of the ligand or the active side of the test ligand that can bind to the target protein receptor (Meng et al., 2022)

CONCLUSIONS

Increasing ethanol concentration increases phenolics, flavonoids, and antioxidant activity. EP5 has the highest total phenolics and flavonoids of 24.978 mgGAE/g and 42.97 mgQE/g, respectively, with an IC_{50} value of 8.263 ppm. The results of Docking on 37 test compounds carried out obtained eight compounds that have good interactions with the NADPH Oxidase protein receptor (PDBid: 2CDU), including kaempferol-3-rhamnoside, meperidine, apigenin-7-O-glucoside, 2-keto benzothiazole 54, methyl propanoic acid, salicyloylaminotriazole, salicylihalamide A and gibberellin A7.

ACKNOWLEDGEMENTS

We sincerely express our gratitude to Universitas Jambi for the research funding provided through the 2024 PNBP Collaboration Scheme (Contract No. 272/UN21.11/PT.01.05).

REFERENCES

Abdul-Hammed, M., Adedotun, I. O., Falade, V. A., Adepoju, A. J., Olasupo, S. B., & Akinboade, M. W. (2021). Target-based drug discovery, ADMET profiling and bioactivity studies of antibiotics as potential inhibitors of SARS-CoV-2 main protease (Mpro). *VirusDisease*, *32*(4), 642–656. https://doi.org/10.1007/s13337-021-00717-z

Acosta-Otálvaro, E., Domínguez-Perles, R., Mazo-Rivas, J. C., & García-Viguera, C. (2022). Bioavailability and radical scavenging power of phenolic compounds of cocoa and coffee mixtures. *Food Science and Technology International*, *28*(6), 514–523. https://doi.org/10.1177/10820132211023258

Alseekh, S., Aharoni, A., Brotman, Y., Contrepois, K., D'Auria, J., Ewald, J., C. Ewald, J., Fraser, P. D., Giavalisco, P., Hall, R. D., Heinemann, M., Link, H., Luo, J., Neumann, S., Nielsen, J., Perez de Souza, L., Saito, K., Sauer, U., Schroeder, F. C., … Fernie, A. R. (2021). Mass spectrometry-based metabolomics: a guide for annotation, quantification and best reporting practices. *Nature Methods*, *18*(7), 747–756. https://doi.org/10.1038/s41592-021-01197-1

Amilia, A. N., & Kustiawan, P. M. (2024). Antioxidant and antibacterial activity of extract combination from *Sonneratia alba* and *Heterotrigona itama* Propolis. *Indonesian Journal of Pharmaceutical Science and Technology, 6*(3), 1–7.

Arief, I., & Hairunnisa, H. (2022). Profil ADME dari entitas molekul baru yang disetujui oleh FDA Tahun 2021: suatu kajian in silico. *Jambura.J.Chem*, *4*(2), 1–11. https://doi.org/10.34312/jambchem.v4i2.15257

Behl, T., Kumar, K., Brisc, C., Rus, M., Nistor-Cseppento, D. C., Bustea, C., Aron, R. A. C., Pantis, C., Zengin, G., Sehgal, A., Kaur, R., Kumar, A., Arora, S., Setia, D., Chandel, D., & Bungau, S. (2021). Exploring the multifocal role of phytochemicals as immunomodulators. *Biomedicine and Pharmacotherapy*, *133*, 110959. https://doi.org/10.1016/j.biopha.2020.110959

Boukarai, Y., Khalil, F., & Bouachrine, M. (2017). QSAR study of flavonoid derivatives as in vitro inhibitors agents of aldose reductase (ALR2) enzyme for diabetic complications. *Journal of Materials and Environmental Science*, *8*(5), 1532–1545.

Chairunisa, F., Safithri, M., & Andrianto, D. (2023). Molecular docking of red betel leaf bioactive compounds (*Piper crocatum*) as lipoxygenase inhibitor. *Indonesian Journal of Pharmaceutical Science and Technology*, *10*(2), 90–103. https://doi.org/https://doi.org/10.24198/ijpst.v10i2

Dettmer, K., Aronov, P. A., & Hammock, B. D. (2009). Mass spectrometry-based metabolomics. *Neuron*, *61*(1), 1–7.

Do, Q. D., Angkawijaya, A. E., Tran-Nguyen, P. L., Huynh, L. H., Soetaredjo, F. E., Ismadji, S., & Ju, Y. H. (2014). Effect of extraction solvent on total phenol content, total flavonoid content, and antioxidant activity of *Limnophila aromatica*. *Journal of Food and Drug Analysis*, *22*(3), 296–302. https://doi.org/10.1016/j.jfda.2013.11.001

Elkordy, A. A., Haj-Ahmad, R. R., Awaad, A. S., & Zaki, R. M. (2021). An overview on natural product drug formulations from conventional medicines to nanomedicines: past, present and future. *Journal of Drug Delivery Science and Technology*, *63*(February). https://doi.org/10.1016/j.jddst.2021.102459

Hasan, R., Herowati, R., & Widodo, G. P. (2023).

Molecular docking and pharmacokinetic prediction of potential compounds from *Luffa acutangula* as antidiabetic candidates. *PHARMACY: Jurnal Farmasi Indonesia (Pharmaceutical Journal of Indonesia)*, *20*(1), 71. https://doi.org/10.30595/pharmacy.v0i0.16066

Hassanpour, S. H., & Doroudi, A. (2023). Review of the antioxidant potential of flavonoids as a subgroup of polyphenols and partial substitute for synthetic antioxidants. *Avicenna Journal of Phytomedicine*, *13*(4), 354–376. https://doi.org/10.22038/AJP.2023.21774

Heriyanti, Putri, Y. E., Irawan, H., Raza'i, T. S., Tarigan, I. L., Kartika, E., Ichwan, B., & Latief, M. (2024). Encapsulation of ethanol extract perepat leaves (*Sonneratia alba*) leaves with maltodextrin coating as an antioxidant functional food candidate. *Indonesian Food Science and Technology Journal*, *7*(2), 193–201. https://doi.org/10.22437/ifstj.v7i2.34013

Ivanović, V., Rančić, M., Arsić, B., & Pavlović, A. (2020). Lipinski's rule of five, famous extensions and famous exceptions. *Chemia Naissensis*, *3*(1), 171–181. https://doi.org/10.46793/chemn3.1.171i

Joosten, R. P., & Lütteke, T. (2017). Carbohydrate 3D structure validation. *Current Opinion in Structural Biology*, *44*, 9–17. https://doi.org/10.1016/j.sbi.2016.10.010

Latief, M., Nelson, N., Amanda, H., Tarigan, I. L., & Aisyah, S. (2020). Potential tracking of cytotoxic activities of mangrove perepate (*Sonneratia alba*) root extract as an anti-cancer candidate. *Pharmacology and Clinical Pharmacy Research*, *5*(2), 48–55. https://doi.org/10.15416/pcpr.v5i2.26790

Latief, M., Utami, A., Fadhilah, N., Bemis, R., Amanda, H., Heriyanti, Rahayu, M. A., Yusnaidar, Syahri, W., & Muhaimin. (2018). Antioxidant activity from perepat plant (*Sonneratia alba*) ethanol leaf extract with CAP-e methods to overcome oxidative stress in thallasemia. *Journal of Pharmaceutical Sciences and Research*, *10*(9), 2160–2162.

Liu, J., Meng, J., Li, R., Jiang, H., Fu, L., Xu, T., Zhu, G. Y., Zhang, W., Gao, J., Jiang, Z. H., Yang, Z. F., & Bai, L. P. (2022). Integrated network pharmacology analysis, molecular docking, LC-MS analysis and bioassays revealed the potential active ingredients and underlying mechanism of *Scutellariae radix* for COVID-19. *Frontiers in Plant Science*, *13*,1–20. https://doi.org/10.3389/fpls.2022.988655

Liu, Y., Liang, S., Shi, D., Zhang, Y., Bai, C., & Ye, R. D. (2023). A predicted structure of NADPH Oxidase 1 identifies key components of ROS generation and strategies for inhibition. *PLoS ONE*, *18*(5 May). https://doi.org/10.1371/journal.pone.0285206

Meng, X.-Y., Zhang, H.-X., Mezei, M., & Cui, M. (2022). Molecular docking: a powerful approach for structure based drug discovery. *International Journal of Pharmaceutical Sciences Review and Research*, *77*(2), 146–157. https://doi.org/10.47583/ijpsrr.2022.v77i02.029

Mhya, D. H., Jakwa, A. G., & Agbo, J. (2023). In silico analysis of antioxidant phytochemicals with potential NADPH oxidase inhibitory effect. *Journal of Health Science and Medical Research*, *41*(2), 1–16. https://doi.org/10.31584/jhsmr.2022912

Moldogazieva, N. T., Mokhosoev, I. M., Feldman, N. B., & Lutsenko, S. V. (2018). ROS and RNS signalling: adaptive redox switches through oxidative/nitrosative protein modifications. *Free Radical Research*, *52*(5), 507–543. https://doi.org/10.1080/10715762.2018.1457217

Neha, K., Haider, M. R., Pathak, A., & Yar, M. S. (2019). Medicinal prospects of antioxidants: A review. *European Journal of Medicinal Chemistry*, *178*, 687–704. https://doi.org/10.1016/j.ejmech.2019.06.010

Pražnikar, J., Tomić, M., & Turk, D. (2019). Validation and quality assessment of macromolecular structures using complex network analysis. *Scientific Reports*, *9*(1), 1–11. https://doi.org/10.1038/s41598-019-38658-9

Santana, K., do Nascimento, L. D., Lima e Lima, A., Damasceno, V., Nahum, C., Braga, R. C., & Lameira, J. (2021). Applications of virtual screening in bioprospecting: facts, shifts, and perspectives to explore the chemo-structural diversity of natural products. *Frontiers in Chemistry*, *9*(April). https://doi.org/10.3389/fchem.2021.662688

Sarno, Suwignyo, R. A., Dahlan, Z., Munandar, Ridho, M. R., Aminasih, N., Harmida, Armanto, M. E., & Wildayana, E. (2017). Short communication: the phenology of *Sonneratia alba* J. Smith in berbak and sembilang national park, South Sumatra, Indonesia. *Biodiversitas*, *18*(3), 909–915. https://doi.org/10.13057/biodiv/d180307

Sidoryk, K., Jaromin, A., Filipczak, N., Cmoch, P., & Cybulski, M. (2018). Synthesis and antioxidant activity of caffeic acid derivatives. *Molecules*, *23*(9), 1–12. https://doi.org/10.3390/molecules23092199

Sies, H., & Jones, D. P. (2020). Reactive oxygen species (ROS) as pleiotropic physiological signalling agents. *Nature Reviews Molecular Cell Biology*, *21*(7), 363–383. https://doi.org/10.1038/s41580-020-0230-3

Silvia, R., Wahyuni, W. T., Rohaeti, E., Aisyah, S.,

Septaningsih, D. A., Karomah, A. H., & Rafi, M. (2024). LC-HRMS-Based metabolomics approach reveals antioxidant compounds from *Centella asiatica* leaves extracts. *Indonesian Journal of Chemistry*, *24*(6), 1861–1869. https://doi.org/10.22146/ijc.90782

Taamalli, A., Arráez-Román, D., Abaza, L., Iswaldi, I., Fernández-Gutiérrez, A., Zarrouk, M., & Segura-Carretero, A. (2015). LC-MS-based metabolite profiling of methanolic extracts from the medicinal and aromatic species *Mentha pulegium* and *Origanum majorana*. *Phytochemical Analysis*, *26*(5), 320–330. https://doi.org/10.1002/pca.2566

Thafar, M., Raies, A. Bin, Albaradei, S., Essack, M., & Bajic, V. B. (2019). Comparison study of computational prediction tools for drug-target binding affinities. *Frontiers in Chemistry*, *7*(November), 1–19. https://doi.org/10.3389/fchem.2019.00782

Tungmunnithum, D., Thongboonyou, A., Pholboon, A., & Yangsabai, A. (2018). Flavonoids and other phenolic compounds from medicinal plants for pharmaceutical and medical aspects: an overview. *Medicines*, *5*(3), 93. https://doi.org/10.3390/medicines5030093

Vaou, N., Stavropoulou, E., Voidarou, C., Tsakris, Z., Rozos, G., Tsigalou, C., & Bezirtzoglou, E. (2022). Interactions between medical plant-derived bioactive compounds: focus on antimicrobial combination effects. *Antibiotics*, *11*(8), 1–23. https://doi.org/10.3390/antibiotics11081014